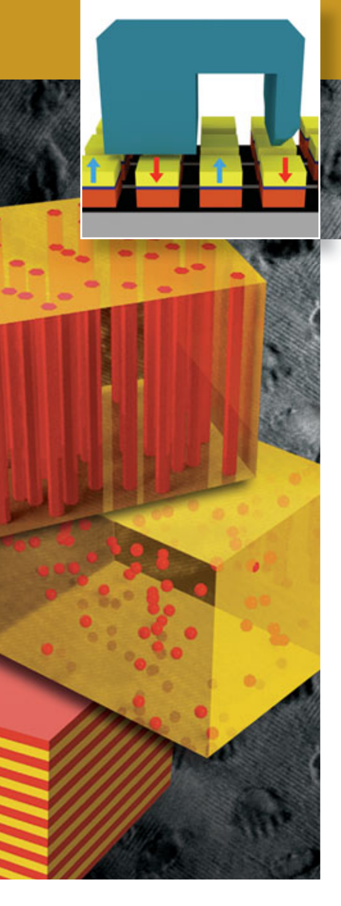

Multiferroic magnetoelectric nanostructures for novel device applications

Jia-Mian Hu, Tianxiang Nan, Nian X. Sun, and Long-Qing Chen

Multiferroic magnetoelectric nanostructures with coupled magnetization and electric polarization across their interfaces have stimulated intense research activities over the past decade. Such interface-based magnetoelectric coupling can be exploited to significantly improve the performance of many devices such as memories, tunable radio-frequency/microwave devices, and magnetic sensors. In this article, we introduce a number of current or developing technologies and discuss their limitations. We describe how the use of magnetoelectric nanostructures can overcome these limitations to optimize device performance. We also present challenges that need to be addressed in pursuing practical applications of magnetoelectric devices.

Multiferroic magnetoelectric nanostructures

Many of today's technological challenges require integration of two or more monolithic material components. Much attention has therefore been paid to the study of interfacial coupling between individual components in composite material systems,[1,2] where new functionalities can arise from coupling among different variables (order parameters) across the interfaces (see the Introductory article in this issue). In particular, in composite nanostructures with relatively large numbers of interfaces, one can utilize these new functionalities to achieve ultimate performance in a device.

One good example is multiferroic magnetoelectric nanostructures, with magnetic and ferroelectric materials integrated at the nanoscale. **Figure 1** shows a nanostructure with juxtaposed magnetic and ferroelectric layers. Across the interface, electric polarization in the ferroelectric layer can be coupled to the magnetization in the magnet, based on the interplay among the lattice, charge, spin, and orbit degrees of freedom achieved typically through the exchange of certain type(s) of potential energy, such as mechanical, electric, and magnetic. Such coupled polarization and magnetization further enable an electrically tunable magnetization or a magnetically tunable polarization, known as converse and direct magnetoelectric coupling, respectively. In this article, we review several novel device prototypes based on interface-based magnetoelectric coupling and provide a brief outlook. Details of recent progress in multiferroic magnetoelectric nanostructures can be found in existing review articles (e.g., References 3–6).

Ultrahigh-density magnetic memories

Based on converse magnetoelectric coupling in multiferroic magnetoelectric nanostructures, the magnetization is switched with an electric field (via, strain[7–12] or exchange bias[13–18] across the interface) rather than a current. This property can be exploited to lift the obstacles now limiting the storage densities of magnetic memories.

Ultrahigh-density hard disk drive

The density limit for a hard disk drive (HDD) is set by the thermal stability of one storage unit that consists of a number of magnetic grains (typically 50–100) in a granular recording medium.[19] This density limit is about 1 Tb in^{-2} for state-of-the-art perpendicular recording technology, where the bit information (i.e., 0 and 1) is represented by the polarity of a magnetization aligning perpendicularly to the plane of the recording medium.[20] To achieve higher area density, the thermal stability of one storage unit, expressed as K_uV_m/k_BT

Jia-Mian Hu, The Pennsylvania State University, USA; juh34@psu.edu
Tianxiang Nan, Northeastern University, USA; nan.t@husky.neu.edu
Nian X. Sun, Northeastern University, USA; n.sun@neu.edu
Long-Qing Chen, The Pennsylvania State University, USA; lqc3@psu.edu
DOI: 10.1557/mrs.2015.195

© 2015 Materials Research Society

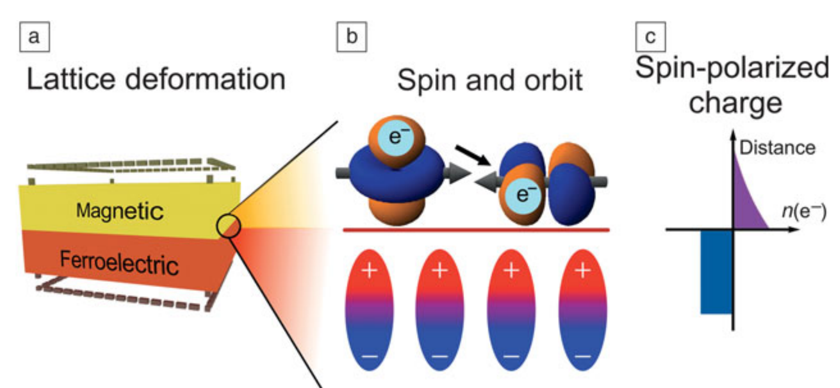

Figure 1. Interplay among lattice, spin, orbit, and charge degrees of freedom across a magnetic–ferroelectric interface induces coupled magnetization and electric polarization. (a) Lattice deformation (strain) can act over a long spatial scale. (b) Polarization charges in the ferroelectric region can attract or repel spin-polarized electrons in the interface region of the magnet, as schematically shown in (c) by the density of spin-polarized electrons, $n(e^-)$, in the case where electrons are attracted to the interface. Accordingly, interfacial magnetism can be modulated based on electrically induced changes in interfacial spin polarization and interfacial orbital configuration.

(where K_u is the uniaxial magnetic anisotropy energy potential, V_m is the effective volume of the storage unit that contributes to magnetic energy, k_B is the Boltzmann constant, and T is the temperature in Kelvin), must be enhanced.[19]

The first approach to enhancing thermal stability is by utilizing perpendicular recording media with higher K_u values. However, the magnetic coercive field (H_c) would also become higher and eventually go beyond the available write magnetic field. Write assist is therefore required to reduce H_c momentarily. For example, an electric field can be utilized to assist magnetization reversal (i.e., electrically assisted magnetic recording [EAMR])[8,21] by reducing H_c in a single magnetic thin film[22] or, more efficiently, in a recording medium based on multiferroic magnetoelectric nanostructures.[8] In these nanostructures, marked reductions of H_c have been observed[3,23] during electrically driven magnetization switching due to the associated large change in magnetic anisotropy. In particular, a strain-mediated, electrically driven reduction in perpendicular magnetic anisotropy (and/or H_c) has recently been observed in an $L1_0$-ordered (a type of face-centered cubic-based-ordered structure) FePt film,[24] one of the promising candidates for practical perpendicular recording media,[25] and in an ultrathin (1.1-nm-thick) $Co_{20}Fe_{60}B_{20}$ film;[26] both are grown on top of a $Pb(Mg_{1/3}Nb_{2/3})_{0.7}Ti_{0.3}O_3$ (PMN-PT) substrate.

Compared to another emerging technology of heat-assisted magnetic recording (HAMR)[27,28] that involves the use of heat from a focused laser beam to reduce H_c, EAMR is much easier to achieve, as it does not require the complex integration of optical, electronic, and magnetic device components in write heads, and therefore can potentially lead to higher storage densities. **Figure 2**a schematically shows one possible setup of EAMR, where a horizontal multiferroic magnetoelectric nanostructure (i.e., juxtaposed nanometer-thick magnetic and ferroelectric films) is considered as the recording medium.

The second approach to enhancing thermal stability is to increase the effective volume of a storage unit (i.e., V_m). For example, it is possible to replace the continuous magnetoelectric composite thin films in Figure 2a with high-density bit-patterned arrays of isolated multiferroic magnetoelectric nanoislands, or bit-patterned magnetoelectric media (BPMeM), as shown in Figure 2b. In this case, each magnetic island represents one storage unit, and the entire volume of the island (V_i) can contribute to the magnetic anisotropy energy (i.e., $V_m = V_i$). More promisingly, purely electric-field-driven 90° and 180° perpendicular magnetization switching have recently been computationally demonstrated in BPMeM using phase-field simulations,[29,30] indicating the possibility of achieving electrically driven magnetic recording (EDMR) under zero magnetic fields (hence without requiring the write coil; see Figure 2b). This EDMR technology can enable ultrahigh-density HDD benefiting from both the much simpler structure and the much lower heat dissipation requirement. (Ideally, there should be no leakage current during writing.)

Ultrahigh-density magnetic random-access memory

Magnetic random-access memory (MRAM) is one of the most promising types of "universal memory"[31,32] that has the potential to replace static random-access memory (SRAM)

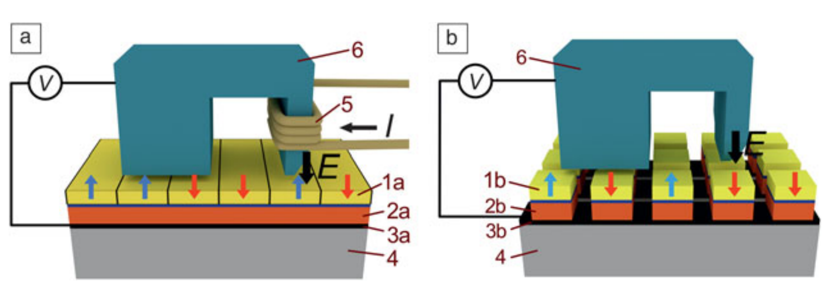

Figure 2. Schematics of (a) electrically assisted magnetic recording, where an electric field (E) is generated across the storage unit by applying a voltage (V) through the write head and an electrode layer underneath the ferroelectric layer. (b) Possible electrically driven magnetic recording under zero magnetic field in high-density arrays of magnetic–ferroelectric nanoislands, namely, bit-patterned magnetoelectric media, where the electric field is selectively applied across the isolated storage unit through the write head and the patterned bottom electrode. Perpendicularly magnetized recording media are considered in all cases, with the arrows indicating magnetization orientations. For simplicity, only the principle of the writing process is shown. (a) Prepared on the basis of Reference 21. Magnetic and ferroelectric thin films in (a) (1a and 2a, respectively) and nanoislands (1b and 2b, respectively) in 2b; (3a) thin-film and (3b) patterned electrode underlayer in 2a and 2b, respectively; (4) substrate; (5) write coil; and (6) Yoke/return pole. Note: I, current.

as the cache memory of the central processing unit, dynamic random-access memory (DRAM) as the principal working memory, or flash memory for permanent data storage. In state-of-the-art MRAM, magnetization in one of the two magnetic layers (separated by a nonmagnetic layer; see **Figure 3**a) is switched by 180° with a current (I) through spin-transfer torque,[33,34] inducing high and low electrical resistance states for antiparallel and parallel magnetization alignment through giant magnetoresistance[35,36] or tunnel magnetoresistance.[37,38] However, the heat dissipation from the current limits the storage density. Thus, a significant amount of research effort has recently been devoted to reducing the threshold current of triggering magnetization reversal[39] by utilizing, for example, vertical current injection[40–42] or an assisting electric field.[43]

In parallel, switching magnetization with an electric field, because of its negligible heat dissipation, can be exploited for the design of ultrahigh-density MRAM [i.e., magnetoelectric RAM (MeRAM)].[44] For example, using phase-field simulations, a multiferroic magnetoelectric-nanostructure-based MeRAM with an area density of up to 88 Gb in^{-2} was computationally demonstrated.[45] The core unit of such an MeRAM is shown in Figure 3b. During writing, an electric voltage is applied perpendicularly across the nanostructure of a magnetic free layer on top of a ferroelectric layer, and the switching of magnetization in the free layer (M_{free}) is then triggered based on magnetoelectric coupling across the interface. The heat dissipation during this process would be negligible if the ferroelectric were sufficiently insulating. The energy consumption can be estimated as $0.5CV^2$ (where C is the capacitance and V is the driving voltage), that is, the energy required to charge a capacitor. If perfect surface screening of polarization charges in the ferroelectric capacitor is assumed, the energy consumption can be further approximated as $0.5P_rSV$ (where P_r is the remnant polarization, and S is the electrode area, which equals the in-plane size of the magnetic free layer according to Figure 3b).

Taking a juxtaposed 64 nm × 64 nm × 5 nm nickel nanomagnet and a PMN-PT ferroelectric layer as a representative nanostructure, the simulated loop of the change in electrical resistance of the entire magnetoresistive multilayer (ΔR) versus the driving voltage (V) is shown in Figure 3c. The distinct electric resistance states ($\Delta R \approx 2.5\%$) at $V = 0$ are induced by the nonvolatile (i.e., stable in the absence of the driving voltage) almost 90° magnetization switching in the nickel free layer (see Figure 3d), mediated by nonvolatile piezostrains from PMN-PT.[46]

An ultralow energy consumption as low as 0.16 fJ is then estimated, which is almost three orders of magnitude smaller than that of MRAM (~0.1 pJ[47]). The low magnitude of the driving voltage (i.e., ~0.26 V) is also compatible with complementary metal oxide semiconductor (CMOS) platforms. Recent progress in fabricating high-quality PMN-PT thin films of giant piezoelectric response on a silicon substrate[48] provides a solid basis for the experimental demonstration of such an MeRAM device prototype.

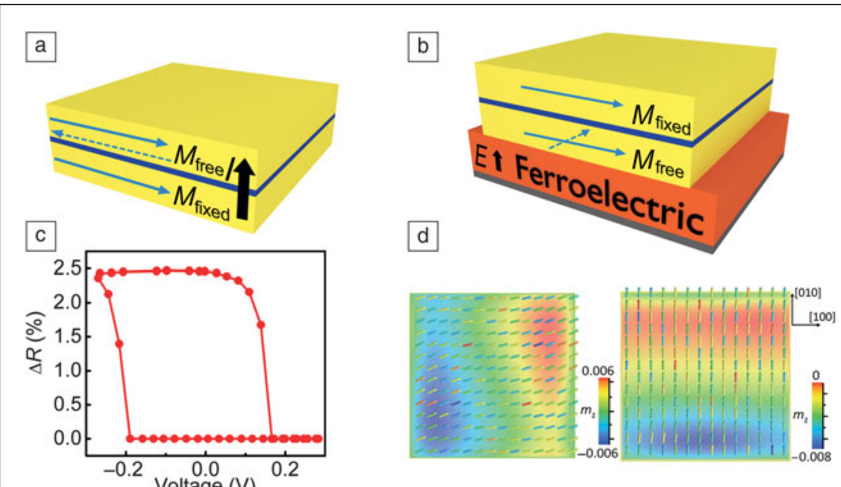

Figure 3. Schematics of (a) a trilayered magnetoresistive element consisting of two magnetic layers (yellow) separated by a nonmagnetic metallic spacer or dielectric tunnel barrier (blue) in magnetic random-access memory (MRAM), where the reversal of magnetization (M_{free}) in the free layer (top) can be driven by a spin-polarized current (I), leading to parallel or antiparallel magnetic alignment between M_{free} and magnetization with a fixed direction (M_{fixed}) in the bottom magnetic layer. (b) A trilayered magnetoresistive element on top of a ferroelectric layer with a bottom electrode for magnetoelectric RAM applications. An electric field (E) applied across the ferroelectric layer can switch the magnetization in its adjacent free layer (M_{free}) by 90° and even 180° according to recent reports (see text). (c) Electrically driven nonvolatile electric resistance switching in a magnetoresistive element consisting of a nickel-free layer and a 2-μm-thick (011) $Pb(Mg_{1/3}Nb_{2/3})_{0.7}Ti_{0.3}O_3$ ferroelectric layer (ΔR, change in electrical resistance). (d) In-plane magnetization vector distributions in the nickel corresponding to the high- (left) and low- (right) resistance states under zero voltages. m_z indicates the out-of-plane component of the normalized magnetization. (c) Adapted from Reference 45. (d) Reproduced with permission from Reference 45. © 2011 Nature Publishing Group.

Furthermore, strain-mediated electrically driven full 180° magnetization switching has recently been proposed for horizontal multiferroic magnetoelectric nanostructures.[30,49–51] On one hand, this full magnetization switching would enhance the magnitude of the electric resistance change of the magnetoresistive multilayer to achieve a higher signal-to-noise ratio. On the other hand, it would significantly enhance the reliability of the proposed MeRAM, because the proposed 180° magnetization switching takes place between the two degenerate directions of one built-in magnetic easy axis in the nanomagnet. In this case, the switched magnetization would remain stable even when the piezostrains were completely relaxed.

The proposed MeRAM concept has also been demonstrated in a $BiFeO_3$-based multiferroic magnetoelectric nanostructure,[18] specifically a $Co_{0.9}Fe_{0.1}$/Cu/$Co_{0.9}Fe_{0.1}$ metallic multilayer grown on top of the $BiFeO_3$ film with a periodic, two-variant ferroelectric domain pattern. An in-plane net magnetization reversal driven by an out-of-plane voltage in the $Co_{0.9}Fe_{0.1}$ free

layer, mediated by exchange coupling between local ferroelectric and magnetic domains across the interface, was directly observed by x-ray magnetic circular dichroism photoemission electron microscopy. Such net magnetization reversal further leads to nonvolatile changes in the electric resistance of the metallic multilayer ($\Delta R \approx 1.4\%$). This is also the first experimental demonstration of an MeRAM prototype based on multiferroic magnetoelectric nanostructures, notably under zero testing magnetic fields. A higher change in electric resistance would appear if a full reversal of uniform magnetization (i.e., single-domain magnet) could be achieved. Particularly, lower power consumption, higher device reliability, and CMOS compatibility could be achieved simultaneously if both the magnitude of the driving voltage (6~7 V) and the leakage current in the $BiFeO_3$ film could be reduced to some extent.

In the MeRAM prototypes discussed so far, an additional ferroelectric layer was integrated with the magnetoresistive multilayer. It is also possible to directly replace the nonmagnetic spacer layer in the magnetoresistive multilayer with an ultrathin (1–2 nm) ferroelectric layer, creating a multiferroic tunnel junction (MFTJ).[52,53] Compared to MeRAM, an MFTJ is simpler in structure, which could be beneficial for achieving an even higher storage density, but reliability might be an issue because of the higher probability of dielectric breakdown in such ultrathin ferroelectrics.

In addition, the working principle of an MFTJ is based not on electrically driven magnetization switching, but on electrically modulated spin-polarized charges across the interfaces. Specifically, by electrically reversing the polarization of the ferroelectric tunnel barrier, the densities of interfacial spin-polarized charges and subsequently the interfacial spin-polarization (noted as η_1 and η_2) in two adjacent magnetic electrodes can be modulated through, for instance, spin-dependent screening.[54] As a result, the tunnel magnetoresistance ratio [$= 2\eta_1\eta_2/(1 - \eta_1\eta_2)$] can be controlled electrically.[55–57]

Furthermore, the tunnel electroresistance, which is a polarization-reversal-triggered electric resistance change that can be observed in any ultrathin ferroelectric capacitor (also known as a ferroelectric tunnel junction [FTJ]), could be dramatically enhanced in an all-oxide MFTJ with multiferroic complex oxide interfaces such as $La_{1-x}A_xMnO_3/BaTiO_3$ (A = Sr, Ca).[58–60] More information on the principles and progress of such MFTJs and FTJs can be found in recent review articles,[61–63] including one in *MRS Bulletin*.[61]

Ultralow-power tunable radio-frequency/microwave magnetic devices

Tunable radio-frequency (RF)/microwave magnetic devices, such as tunable inductors, tunable filters, tunable resonators, and phase shifters, have been widely deployed in aircraft, satellites, and portable communication systems.[5,64,65] Such tunable RF/microwave magnetic devices typically operate on the basis of a dramatic change in permeability at approximately the ferromagnetic resonance (FMR), which arises from the precessional motion of magnetization in an external magnetic field. Therefore, a current-driven electromagnet is typically necessary in these devices (see schematic in **Figure 4**a), which, in principle, makes them energy-consuming, bulky, noisy, and difficult for on-chip integration. In multiferroic magnetoelectric nanostructures, the permeability of the magnetic phase can alternatively be tuned by a non-power-dissipating electric field mediated by electrostrains, enabling electrically tunable RF/microwave magnetic devices with ultralow power consumption. An electric field is also easy to generate and localize on a chip, which is beneficial for device miniaturization.

For example, in a horizontal magnetoelectric nanostructure consisting of a 20-nm-thick $Co_{20}Fe_{60}B_{20}$ (CoFeB) film grown on top of a 500-μm-thick (011)-oriented PMN-PT layer (see Figure 4b), a small electric field of 1.5 kV cm^{-1} applied across the nanostructure can shift the FMR frequency of the CoFeB film by up to 2.3 GHz (see Figure 4c),[66] based on an

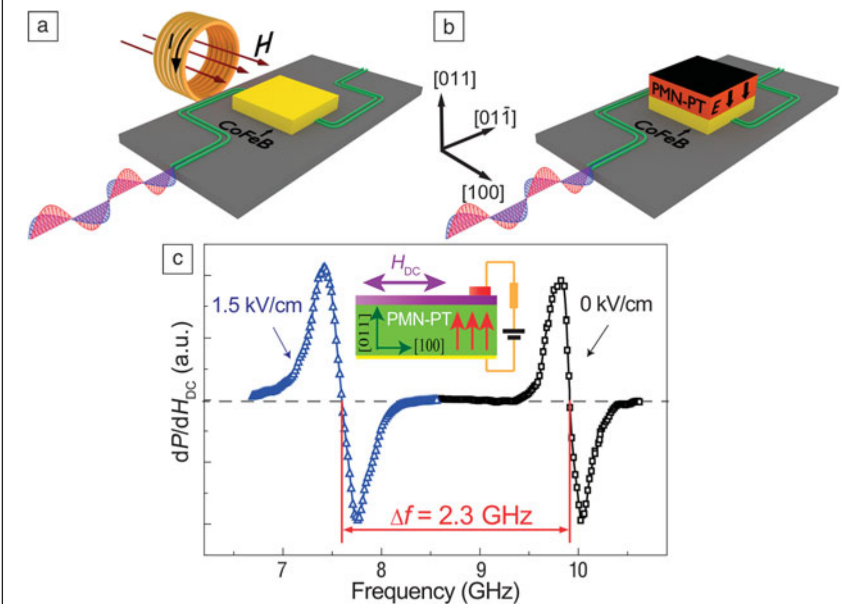

Figure 4. Experimental setup of ferromagnetic resonance measurement for demonstrating the working principles of (a) magnetically and (b) electrically tunable radio-frequency/microwave magnetic devices, where a single-layer magnetic thin film (e.g., $Co_{20}Fe_{60}B_{20}$ [CoFeB]) or a bilayered magnetoelectric nanostructure is laid face down on an S-shaped coplanar waveguide (CPW). The CPW generates a microwave magnetic field to excite magnetization precession in CoFeB. A DC testing magnetic field (H_{DC}) of 720 Oe is applied along the [100] direction in both cases (not shown). (c) First derivative of the absorption power (P) with respect to H_{DC} as a function of the frequency of the microwave magnetic field. The resonance frequencies that are determined by the intersection of the spectra and the baseline (dashed line) can be modulated by an applied electric field. The ferroelectric layer is $Pb(Mg_{1/3}Nb_{2/3})_{0.71}Ti_{0.3}O_{0.29}$ (PMN-PT). (b) Adapted with permission from Reference 65. © 2014 Royal Society Publishing. (c) Adapted with permission from Reference 66. © 2013 Wiley-VCH.

electrostrain-induced change in permeability.[5] Although the use of magnetic alloys (e.g., CoFeB and FeGaB[67]) with large magnetostriction can lead to high strain-mediated electrical tunability, the high microwave loss of these alloy materials is an important issue. Low-loss magnetic ferrites such as epitaxial single-crystal yttrium iron garnet (YIG) have been widely used in magnetically tunable RF/microwave devices, but their smaller magnetostriction leads to lower electrical tunability. Nevertheless, it is possible to achieve reasonably high electrical tunability in YIG-based magnetoelectric nanostructures with sharp and elastically coherent interfaces. For instance, in a high-quality multilayered magnetoelectric nanostructure of YIG (300-nm-thick)–Pt (30-nm-thick)–$(Ba,Sr)TiO_3$ (BSTO, 1-μm-thick)–Pt (50-nm-thick) grown on a single-crystal gadolinium gallium garnet substrate,[68] a maximum electrical tunability of FMR of above 2 MHz V^{-1} can be achieved at 25 V, which is nearly one order of magnitude larger than that in a bulk heterostructure with a mechanically bonded YIG (7-μm-thick) layer and BSTO ceramic slab (500-μm-thick).[69]

Ultralow-cost magnetic field sensors

Ultrasensitive and high-spatial-resolution magnetic field sensors are critically important to noninvasive medical imaging and diagnosis, such as magnetoencephalography (MEG, which detects magnetic fields of the brain to analyze neural activities), cardiological diagnosis, and magnetogastrography, which detects magnetic fields of the stomach. Given that the magnetic fields produced by human organs are typically weak, ranging from 10 fT to 1 pT,[70,71] and have low frequencies (below 10^3 Hz),[72] magnetic field sensors with sub-picotesla sensitivity in this frequency range are desired. This leaves no option but to use ultrasensitive magnetic field sensors based on high-density arrays of a superconducting quantum interference device (SQUID), which, however, require expensive and cumbersome cryogenic systems (e.g., see a practical MEG system from the brain mapping center of University of Pittsburgh Medical Center at www.meg-brain-mapping.pitt.edu). Thus, it is imperative to develop a novel low-cost magnetic field sensor whose sensitivity is comparable to that of a SQUID-based sensor.

Multiferroic-magnetoelectric-composite-based magnetic field sensors, with ultralow cost and compact size,[73] have been demonstrated as among the most promising candidates. These magnetoelectric sensors allow a direct transformation (i.e., without requiring source current) of a weak AC magnetic field signal into a voltage signal over a broad temperature range (e.g., from –35°C to 85°C; see Reference 74) through a strain-mediated direct magnetoelectric coupling (i.e., magnetically tunable polarization).[75–77] In particular, the sensitivity of magnetoelectric sensors based on bulk magnetoelectric composites[72] can become comparable to that of a SQUID-based sensor if the frequency of the target magnetic field is equal or close to the electromechanical resonance frequency (typically 10^4–10^5 Hz) of the constituent ferroelectric/piezoelectric material.[78]

However, it is difficult to utilize bulk magnetoelectric composites to fabricate high-density magnetoelectric sensor arrays for biomedical use.[79] More importantly, the sensitivity of existing magnetoelectric sensor prototypes is insufficient to detect low-frequency (below 10^3 Hz) AC magnetic fields for the following three reasons. First, the strain-mediated direct magnetoelectric response is typically low (resulting in weak magnetically induced voltage signals) if the frequency of the target AC magnetic field is far from electromechanical resonance. Second, the noise level increases significantly with decreasing frequency f because of the $1/f$ noise,[80,81] as in other types of magnetic field sensors. Third, the externally applied DC bias magnetic field, commonly used to set the piezomagnetic coefficient at a maximum to maximize the direct magnetoelectric coupling,[3,82] creates an additional noise source. The use of such an external bias magnetic field in high-density magnetoelectric sensor arrays would also lead to crosstalk among neighboring sensors and, hence decrease the spatial resolution.

Recently, on a silicon cantilever substrate, a horizontal magnetoelectric nanostructure consisting of a magnetic multilayer of $Ta/Cu/Mn_{70}Ir_{30}/FeCoSiB$ (or $Fe_{50}Co_{50}$) grown on a 2-μm-thick piezoelectric AlN layer was fabricated.[83] Because of the tightly bonded interfaces at the nanoscale (see **Figure 5**a) and the relieved mechanical constraint from the substrate in the cantilever geometry (i.e., the multilayer is only clamped

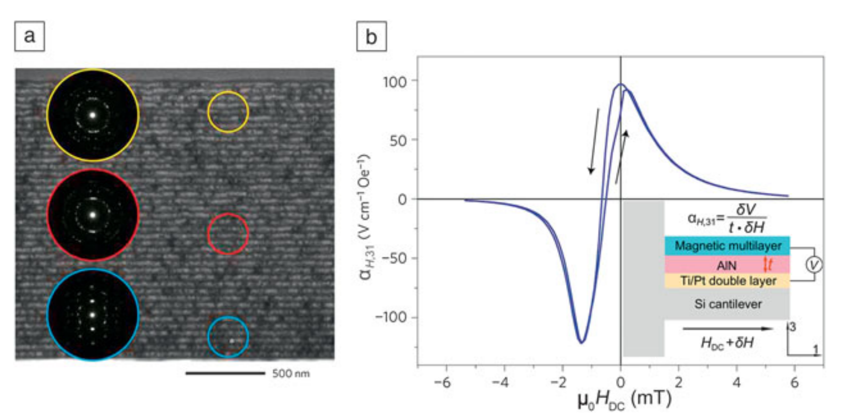

Figure 5. (a) Cross-sectional transmission electron microscope bright-field image of a horizontal magnetoelectric nanostructure consisting of a $Ta/Cu/Mn_{70}Ir_{30}/Fe_{50}Co_{50}$ multilayer deposited on an AlN layer on a silicon cantilever substrate, with selected-area electron diffraction patterns of different sample areas. The asterisk inside the blue circle on the right indicates the area next to the multilayer/AlN interface. (b) The magnetoelectric voltage coefficient $\alpha_{H,31}$ as a function of the DC bias magnetic field ($\mu_0 H_{DC}$, where the prefactor μ_0 is the vacuum permeability) in the magnetoelectric nanostructure based on a $Ta/Cu/Mn_{70}Ir_{30}/Fe_{70.2}Co_{7.8}Si_{12}B_{10}$ multilayer under an excitation magnetic field (δH) with a frequency of 1197 Hz. The inset schematically shows the sample geometry and the definition of $\alpha_{H,31}$, where δV is the induced voltage and t is the thickness of the AlN layer. Adapted with permission from Reference 83. © 2012 Nature Publishing Group.

on one end, see the inset of Figure 5b), a significant amount of magnetic-field-induced strain can be obtained and transferred efficiently to the AlN, leading to a high magnetoelectric coefficient $\alpha_{H,31}$ (= dE_3/dH_1) of over 100 V cm^{-1} Oe^{-1} at a resonance frequency of 1197 Hz, which is close to the desirable frequency range below 10^3 Hz. Here, E_3 and H_1 indicate the induced electric field and applied magnetic field along the out-of-plane and in-plane (long axis of the cantilever substrate) directions, respectively. In particular, by exploiting the exchange bias field between the antiferromagnetic $Mn_{70}Ir_{30}$ and the ferromagnetic FeCoSiB (or $Fe_{50}Co_{50}$) in the multilayer as a built-in DC bias magnetic field, a high $\alpha_{H,31}$ value of 96.7 V cm^{-1} Oe^{-1} is obtained under zero externally applied bias magnetic field (Figure 5b), which is beneficial for achieving a low noise level and a high spatial resolution. Indeed, with this built-in bias magnetic field and the high value of $\alpha_{H,31}$, a high sensitivity limit of 10 pT Hz$^{-1/2}$ was achieved at resonance frequency for the FeCoSiB-based magnetoelectric nanostructure. By optimizing the thickness and magnetic domain structure of the FeCoSiB layer, $\alpha_{H,31}$ was recently enhanced to about 430 V cm^{-1} Oe^{-1} at a lower resonance frequency of about 700 Hz,[84] which should lead to an even higher sensitivity.

More recently, a novel nanoelectromechanical systems (NEMS) magnetoelectric resonator consisting of a multilayered AlN/(FeGaB/Al_2O_3) heterostructure on an etched silicon substrate was developed for detecting low-frequency AC magnetic fields.[85] In such an NEMS magnetoelectric resonator, the magnetic field can be sensed not only by electrically detecting the magnetically tunable polarization, where an external or built-in DC bias field is required, as mentioned earlier, but also by electrically detecting the magnetically tunable electromechanical resonance frequency. The latter is based on the ΔE effect[86] (i.e., magnetic-field-induced changes in the Young's modulus of magnetic materials), and these changes are nonzero under zero DC bias magnetic field. Thus, in the latter scenario, a DC bias magnetic field is no longer required. Furthermore, the frequency of the target AC magnetic field does not have to be the same as the electromechanical frequency for the enhanced sensitivity, allowing the detection of a broadband low-frequency AC and even DC magnetic fields.[85] It is also easy to integrate such NEMS resonators with CMOS platforms to fabricate high-density magnetoelectric sensor arrays.

Outlook

The interface-based magnetoelectric coupling in multiferroic magnetoelectric nanostructures is being exploited for many exciting device technologies. Compared to bulk multiferroic magnetoelectric heterostructures, these magnetoelectric nanostructures are easier to integrate on a chip, and their interfaces can be controlled or designed for enhanced magnetoelectric coupling or new functionalities (e.g., MFTJ). Despite the bright future and notable progress, many challenges remain to be overcome before the practical use of these magnetoelectric nanostructures in the mentioned device technologies.

To compete with the complex but very effective HAMR technology, larger electric-field-induced reductions in the perpendicular magnetic anisotropy and magnetic coercive field are desirable for EAMR. This requires further enhancement of the converse magnetoelectric coupling across the magnetic–ferroelectric interface in the layered magnetoelectric composite thin film (shown in Figure 2a), which is challenging because the electric-field-induced strain would be limited by substrate clamping. One promising solution is to exploit interfacial charge-mediated converse magnetoelectric coupling, which can become effective over a long spatial scale (up to tens of nanometers) near the interface through exchange coupling[22] or magnon excitation[87,88] and can become stronger with intervention from interfacial redox reactions.[89–91] A more promising solution is based on high-density arrays of layered magnetic–ferroelectric nanoislands. Such novel magnetoelectric nanostructures were recently predicted to show strong strain-mediated magnetoelectric coupling due to the extraordinarily large (1% and above) electric-field-induced homogeneous strains[29,30] and, in particular, to exhibit a purely electrically driven reversal of uniform magnetization[30] that can be exploited for both high-density HDD (see Figure 2b) and high-density perpendicular MRAM. Both predictions remain to be verified by experiments.

For application as electrically tunable RF/microwave devices, one of the challenges is to develop magnetic materials (most likely, based on ferrites) that simultaneously exhibit low microwave loss and large magnetostriction (for high strain-mediated electrical tunability). A promising approach to achieving greater flexibility for materials selection and design is to exploit interfacial charge-mediated converse magnetoelectric coupling (as recently demonstrated experimentally[92,93]), such that large magnetostriction is no longer necessary.

It is appealing to replace the expensive and bulky SQUID-based magnetic sensor arrays with low-cost and compact-sized magnetoelectric-nanostructure-based magnetic sensor arrays for biomedical imaging and diagnosis. The high sensitivities on the order of pT Hz$^{-1/2}$ for low-frequency ($<10^3$ Hz) magnetic field detection, recently achieved in self-biased multilayered magnetoelectric nanostructures,[83,85] represent important progress, but there is still a long way to go. One of the most immediate needs is to further enhance the low-frequency magnetic field sensitivity to the order of *f*T Hz$^{-1/2}$: a level not far from that of SQUID-based magnetic sensors.[94,95] This should be pursued, on one hand, by enhancing the direct magnetoelectric coupling (e.g., by optimizing the microstructure and interfaces of such multilayered magnetoelectric nanostructures[84] or possibly by operating them in shear mode[96]) and, on the other hand, by reducing the noise level.[97]

Acknowledgments

We gratefully acknowledge our colleagues and collaborators for sharing their insights and contributions, including C.W. Nan, Q.M. Zhang, C.B. Eom, D.G. Schlom, and R. Ramesh.

We especially thank X.X. Cheng for help preparing the schematic figures and M.-C. Lu and M. Liu for helpful discussions. J.-M.H. and L.-Q.C. gratefully acknowledge financial support from the National Science Foundation under Grant DMR-1234096. T.N. and N.X.S. gratefully acknowledge financial support from the Air Force Research Laboratory through Contract FA8650-14-C-5706 and, in part, Contract FA8650-14-C-5705 and from the W.M. Keck Foundation.

References

1. P. Yang, J.-M. Tarascon, *Nat. Mater.* **11**, 560 (2012).
2. H.Y. Hwang, Y. Iwasa, M. Kawasaki, B. Keimer, N. Nagaosa, Y. Tokura, *Nat. Mater.* **11**, 103 (2012).
3. J. Ma, J. Hu, Z. Li, C.-W. Nan, *Adv. Mater.* **23**, 1062 (2011).
4. C.A.F. Vaz, *J. Phys. Condens. Matter* **24**, 333201 (2012).
5. N.X. Sun, G. Srinivasan, *Spin* **2**, 1240004 (2012).
6. S. Fusil, V. Garcia, A. Barthélémy, M. Bibes, *Annu. Rev. Mater. Res.* **44**, 91 (2014).
7. W. Eerenstein, M. Wiora, J.L. Prieto, J.F. Scott, N.D. Mathur, *Nat. Mater.* **6**, 348 (2007).
8. F. Zavaliche, T. Zhao, H. Zheng, F. Straub, M.P. Cruz, P.L. Yang, D. Hao, R. Ramesh, *Nano Lett.* **7**, 1586 (2007).
9. C. Thiele, K. Dörr, O. Bilani, J. Rödel, L. Schultz, *Phys. Rev. B Condens. Matter* **75**, 054408 (2007).
10. J.-M. Hu, C.W. Nan, *Phys. Rev. B Condens. Matter* **80**, 224416 (2009).
11. S. Geprägs, A. Brandlmaier, M. Opel, R. Gross, S.T.B. Goennenwein, *Appl. Phys. Lett.* **96**, 142509 (2010).
12. T.H.E. Lahtinen, K.J.A. Franke, S. van Dijken, *Sci. Rep.* **2**, 258 (2012).
13. Y.-H. Chu, L.W. Martin, M.B. Holcomb, M. Gajek, S.-J. Han, Q. He, N. Balke, C.-H. Yang, D. Lee, W. Hu, Q. Zhan, P.-L. Yang, A. Fraile-Rodriguez, A. Scholl, S.X. Wang, R. Ramesh, *Nat. Mater.* **7**, 478 (2008).
14. S.M. Wu, S.A. Cybart, P. Yu, M.D. Rossell, J.X. Zhang, R. Ramesh, R.C. Dynes, *Nat. Mater.* **9**, 756 (2010).
15. V. Skumryev, V. Laukhin, I. Fina, X. Martí, F. Sánchez, M. Gospodinov, J. Fontcuberta, *Phys. Rev. Lett.* **106**, 057206 (2011).
16. J.T. Heron, M. Trassin, K. Ashraf, M. Gajek, Q. He, S.Y. Yang, D.E. Nikonov, Y.H. Chu, S. Salahuddin, R. Ramesh, *Phys. Rev. Lett.* **107**, 217202 (2011).
17. S.M. Wu, S.A. Cybart, D. Yi, J.M. Parker, R. Ramesh, R.C. Dynes, *Phys. Rev. Lett.* **110**, 067202 (2013).
18. J.T. Heron, J.L. Bosse, Q. He, Y. Gao, M. Trassin, L. Ye, J.D. Clarkson, C. Wang, J. Liu, S. Salahuddin, D.C. Ralph, D.G. Schlom, J. Iniguez, B.D. Huey, R. Ramesh, *Nature* **516**, 370 (2014).
19. H.J. Richter, *J. Phys. D Appl. Phys.* **40**, R149 (2007).
20. Hitachi, Ltd., "Hitachi Achieves Nanotechnology Milestone for Quadrupling Terabyte Hard Drive," available at http://www.hitachi.com/New/cnews/071015a.html. News release. October 17, 2007 (accessed July 2015).
21. Y. Zhou, K. Liu, K. Zhang, E. Schreck, "Electric Field Assisted Magnetic Recording," US Patent 8,023,218 B2 (September 20, 2011).
22. T. Zhou, S.H. Leong, Z.M. Yuan, S.B. Hu, C.L. Ong, B. Liu, *Appl. Phys. Lett.* **96**, 012506 (2010).
23. J. Wang, J. Ma, Z. Li, Y. Shen, Y. Lin, C.W. Nan, *J. Appl. Phys.* **110**, 043919 (2011).
24. W.-C. Tsai, S.-C. Liao, K.-F. Huang, D.-S. Wang, C.-H. Lai, *Appl. Phys. Lett.* **103**, 252405 (2013).
25. J.-U. Thiele, S. Maat, E.E. Fullerton, *Appl. Phys. Lett.* **82**, 2859 (2003).
26. G. Yu, Z. Wang, M. Abolfath-Beygi, C. He, X. Li, K.L. Wong, P. Nordeen, H. Wu, G.P. Carman, X. Han, I.A. Alhomoudi, P.K. Amiri, K.L. Wang, *Appl. Phys. Lett.* **106**, 072402 (2015).
27. R.E. Rottmayer, S. Batra, D. Buechel, W.A. Challener, J. Hohlfeld, Y. Kubota, L. Li, L. Bin, C. Mihalcea, K. Mountfield, K. Pelhos, C. Peng, T. Rausch, M.A. Seigler, D. Weller, X. Yang, *IEEE Trans. Magn.* **42**, 2417 (2006).
28. M.H. Kryder, E.C. Gage, T.W. McDaniel, W.A. Challener, R.E. Rottmayer, J. Ganping, Y.-T. Hsia, M.F. Erden, *Proc. IEEE* **96**, 1810 (2008).
29. J.-M. Hu, T.N. Yang, L.Q. Chen, C.W. Nan, *J. Appl. Phys.* **113**, 194301 (2013).
30. J.-M. Hu, T. Yang, J. Wang, H. Huang, J. Zhang, L.-Q. Chen, C.-W. Nan, *Nano Lett.* **15**, 616 (2015).
31. J. Åkerman, *Science* **308**, 508 (2005).
32. J.G. Zhu, *Proc. IEEE* **96**, 1786 (2008).
33. J.C. Slonczewski, *J. Magn. Magn. Mater.* **159**, L1 (1996).
34. L. Berger, *Phys. Rev. B Condens. Matter* **54**, 9353 (1996).
35. M.N. Baibich, J.M. Broto, A. Fert, F.N. Van Dau, F. Petroff, P. Etienne, G. Creuzet, A. Friederich, J. Chazelas, *Phys. Rev. Lett.* **61**, 2472 (1988).
36. G. Binasch, P. Grünberg, F. Saurenbach, W. Zinn, *Phys. Rev. B Condens. Matter* **39**, 4828 (1989).
37. M. Julliere, *Phys. Lett. A* **54**, 225 (1975).
38. J.S. Moodera, L.R. Kinder, T.M. Wong, R. Meservey, *Phys. Rev. Lett.* **74**, 3273 (1995).
39. A. Brataas, A.D. Kent, H. Ohno, *Nat. Mater.* **11**, 372 (2012).
40. A. Khvalkovskiy, K. Zvezdin, Y. Gorbunov, V. Cros, J. Grollier, A. Fert, A. Zvezdin, *Phys. Rev. Lett.* **102**, 067206 (2009).
41. A. Chanthbouala, R. Matsumoto, J. Grollier, V. Cros, A. Anane, A. Fert, A.V. Khvalkovskiy, K.A. Zvezdin, K. Nishimura, Y. Nagamine, H. Maehara, K. Tsunekawa, A. Fukushima, S. Yuasa, *Nat. Phys.* **7**, 626 (2011).
42. P.J. Metaxas, J. Sampaio, A. Chanthbouala, R. Matsumoto, A. Anane, A. Fert, K.A. Zvezdin, K. Yakushiji, H. Kubota, A. Fukushima, S. Yuasa, K. Nishimura, Y. Nagamine, H. Maehara, K. Tsunekawa, V. Cros, J. Grollier, *Sci. Rep.* **3**, 1829 (2013).
43. W.-G. Wang, M. Li, S. Hageman, C.L. Chien, *Nat. Mater.* **11**, 64 (2012).
44. K.L. Wang, J.G. Alzate, P.K. Amiri, *J. Phys. D Appl. Phys.* **46**, 074003 (2013).
45. J.-M. Hu, Z. Li, L.-Q. Chen, C.-W. Nan, *Nat. Commun.* **2**, 553 (2011).
46. T. Wu, A. Bur, P. Zhao, K.P. Mohanchandra, K. Wong, K.L. Wang, C.S. Lynch, G.P. Carman, *Appl. Phys. Lett.* **98**, 012504 (2011).
47. H. Ohno, *Nat. Mater.* **9**, 952 (2010).
48. S.H. Baek, J. Park, D.M. Kim, V.A. Aksyuk, R.R. Das, S.D. Bu, D.A. Felker, J. Lettieri, V. Vaithyanathan, S.S.N. Bharadwaja, N. Bassiri-Gharb, Y.B. Chen, H.P. Sun, C.M. Folkman, H.W. Jang, D.J. Kreft, S.K. Streiffer, R. Ramesh, X.Q. Pan, S. Trolier-McKinstry, D.G. Schlom, M.S. Rzchowski, R.H. Blick, C.B. Eom, *Science* **334**, 958 (2011).
49. J.J. Wang, J.M. Hu, J. Ma, J.X. Zhang, L.Q. Chen, C.W. Nan, *Sci. Rep.* **4**, 7507 (2014).
50. R.-C. Peng, J.J. Wang, J.-M. Hu, L.-Q. Chen, C.-W. Nan, *Appl. Phys. Lett.* **106**, 142901 (2015).
51. K. Roy, S. Bandyopadhyay, J. Atulasimha, *Sci. Rep.* **3**, 3038 (2013).
52. J.F. Scott, *Nat. Mater.* **6**, 256 (2007).
53. J.P. Velev, C.G. Duan, J.D. Burton, A. Smogunov, M.K. Niranjan, E. Tosatti, S.S. Jaswal, E.Y. Tsymbal, *Nano Lett.* **9**, 427 (2009).
54. S. Zhang, *Phys. Rev. Lett.* **83**, 640 (1999).
55. V. Garcia, M. Bibes, L. Bocher, S. Valencia, F. Kronast, A. Crassous, X. Moya, S. Enouz-Vedrenne, A. Gloter, D. Imhoff, C. Deranlot, N.D. Mathur, S. Fusil, K. Bouzehouane, A. Barthélémy, *Science* **327**, 1106 (2010).
56. S. Valencia, A. Crassous, L. Bocher, V. Garcia, X. Moya, R.O. Cherifi, C. Deranlot, K. Bouzehouane, S. Fusil, A. Zobelli, A. Gloter, N.D. Mathur, A. Gaupp, R. Abrudan, F. Radu, A. Barthélémy, M. Bibes, *Nat. Mater.* **10**, 753 (2011).
57. D. Pantel, S. Goetze, D. Hesse, M. Alexe, *Nat. Mater.* **11**, 289 (2012).
58. J. D. Burton, E.Y. Tsymbal, *Phys. Rev. B Condens. Matter* **80**, 174406 (2009).
59. J.D. Burton, E.Y. Tsymbal, *Phys. Rev. Lett.* **106**, 157203 (2011).
60. Y.W. Yin, J.D. Burton, Y.M. Kim, A.Y. Borisevich, S.J. Pennycook, S.M. Yang, T.W. Noh, A. Gruverman, X.G. Li, E.Y. Tsymbal, Q. Li, *Nat. Mater.* **12**, 397 (2013).
61. E.Y. Tsymbal, A. Gruverman, V. Garcia, M. Bibes, A. Barthélémy, *MRS Bull.* **37**, 138 (2012).
62. V. Garcia, M. Bibes, *Nat. Commun.* **5**, 4289 (2014).
63. Y.W. Yin, M. Raju, W.J. Hu, J.D. Burton, Y.-M. Kim, A.Y. Borisevich, S.J. Pennycook, S.M. Yang, T.W. Noh, A. Gruverman, X.G. Li, Z.D. Zhang, E.Y. Tsymbal, Q. Li, *J. Appl. Phys.* **117**, 172601 (2015).
64. G. Srinivasan, *Annu. Rev. Mater. Res.* **40**, 153 (2010).
65. M. Liu, N.X. Sun, *Philos. Trans. R. Soc. Lond. A* **372**, 20120439 (2014).
66. M. Liu, B.M. Howe, L. Grazulis, K. Mahalingam, T. Nan, N.X. Sun, G.J. Brown, *Adv. Mater.* **25**, 4886 (2013).
67. J. Lou, M. Liu, D. Reed, Y.H. Ren, N.X. Sun, *Adv. Mater.* **21**, 4711 (2009).
68. J. Das, Y.-Y. Song, N. Mo, P. Krivosik, C.E. Patton, *Adv. Mater.* **21**, 2045 (2009).
69. A.B. Ustinov, V.S. Tiberkevich, G. Srinivasan, A.N. Slavin, A.A. Semenov, S.F. Karmanenko, B.A. Kalinikos, J.V. Mantese, R. Ramer, *J. Appl. Phys.* **100**, 093905 (2006).
70. Y. Nakaya, H. Mori, *Clin. Phys. Physiol. Meas.* **13**, 191 (1992).
71. J.P. Wikswo Jr., *IEEE Trans. Appl. Supercond.* **5**, 74 (1995).
72. J. Zhai, Z. Xing, S. Dong, J. Li, D. Viehland, *Appl. Phys. Lett.* **88**, 062510 (2006).
73. C. Israel, N.D. Mathur, J.F. Scott, *Nat. Mater.* **7**, 93 (2008).
74. J.-X. Ye, J.-N. Ma, J. Ma, J.-M. Hu, Z. Li, M. Feng, Q.M. Zhang, C.W. Nan, *J. Appl. Phys.* **116**, 074103 (2014).
75. C.-W. Nan, G. Liu, Y. Lin, H. Chen, *Phys. Rev. Lett.* **94**, 197203 (2005).
76. Z. Li, Y. Wang, Y.H. Lin, C.W. Nan, *Phys. Rev. B Condens. Matter* **79**, 180406 (2009).
77. J. Wang, Z. Li, J. Wang, H. He, C.-W. Nan, *J. Appl. Phys.* **117**, 044101 (2015).
78. M.I. Bichurin, D.A. Filippov, V.M. Petrov, V.M. Laletsin, N. Paddubnaya, G. Srinivasan, *Phys. Rev. B Condens. Matter* **68**, 132408 (2003).
79. H. Greve, E. Woltermann, H.-J. Quenzer, B. Wagner, E. Quandt, *Appl. Phys. Lett.* **96**, 182501 (2010).
80. A.S. Edelstein, G.A. Fischer, *J. Appl. Phys.* **91**, 7795 (2002).

81. N.A. Stutzke, S.E. Russek, D.P. Pappas, M. Tondra, *J. Appl. Phys.* **97**, 10Q107 (2005).
82. Y. Wang, J. Hu, Y. Lin, C.-W. Nan, *NPG Asia Mater.* **2**, 61 (2010).
83. E. Lage, C. Kirchhof, V. Hrkac, L. Kienle, R. Jahns, R. Knochel, E. Quandt, D. Meyners, *Nat. Mater.* **11**, 523 (2012).
84. E. Lage, N.O. Urs, V. Röbisch, I. Teliban, R. Knöchel, D. Meyners, J. McCord, E. Quandt, *Appl. Phys. Lett.* **104**, 132405 (2014).
85. T. Nan, Y. Hui, M. Rinaldi, N.X. Sun, *Sci. Rep.* **3**, 1985 (2013).
86. A. Ludwig, E. Quandt, *IEEE Trans. Magn.* **38**, 2829 (2002).
87. N. Jedrecy, H.J. von Bardeleben, V. Badjeck, D. Demaille, D. Stanescu, H. Magnan, A. Barbier, *Phys. Rev. B Condens. Matter* **88**, 121409 (2013).
88. C.L. Jia, T.L. Wei, C.J. Jiang, D.S. Xue, A. Sukhov, J. Berakdar, *Phys. Rev. B Condens. Matter* **90**, 054423 (2014).
89. K. Leistner, J. Wunderwald, N. Lange, S. Oswald, M. Richter, H. Zhang, L. Schultz, S. Fähler, *Phys. Rev. B Condens. Matter* **87**, 224411 (2013).
90. U. Bauer, L. Yao, A.J. Tan, P. Agrawal, S. Emori, H.L. Tuller, S. van Dijken, G.S.D. Beach, *Nat. Mater.* **14**, 174 (2015).
91. C. Bi, Y. Liu, T. Newhouse-Illige, M. Xu, M. Rosales, J.W. Freeland, O. Mryasov, S. Zhang, S.G.E. te Velthuis, W.G. Wang, *Phys. Rev. Lett.* **113**, 267202 (2014).
92. T. Nan, Z. Zhou, M. Liu, X. Yang, Y. Gao, B.A. Assaf, H. Lin, S. Velu, X. Wang, H. Luo, J. Chen, S. Akhtar, E. Hu, R. Rajiv, K. Krishnan, S. Sreedhar, D. Heiman, B.M. Howe, G.J. Brown, N.X. Sun, *Sci. Rep.* **4**, 3688 (2014).
93. Z. Zhou, B.M. Howe, M. Liu, T. Nan, X. Chen, K. Mahalingam, N.X. Sun, G.J. Brown, *Sci. Rep.* **5**, 7740 (2015).
94. J. Gallop, *Supercond. Sci. Technol.* **16**, 1575 (2003).
95. R.L. Fagaly, *Rev. Sci. Instrum.* **77**, 101101 (2006).
96. M.-C. Lu, L. Mei, D.-Y. Jeong, J. Xiang, H. Xie, Q.M. Zhang, *Appl. Phys. Lett.* **106**, 112905 (2015).
97. Y.J. Wang, J.Q. Gao, M.H. Li, Y. Shen, D. Hasanyan, J.F. Li, D. Viehland, *Philos. Trans. R. Soc. Lond. A* **372**, 20120455 (2014).